International Communications in Heat and Mass Transfer 104 (2019) 1–7

Contents lists available at ScienceDirect

International Communications in Heat and Mass Transfer

journal homepage: www.elsevier.com/locate/ichmt

Microscale sets a fundamental limit to heat transfer

Barak Kashi, Herman D. Haustein*

School of Mechanical Engineering, Faculty of Engineering, Tel Aviv University, Tel Aviv 6997801, Israel

ARTICLE INFO

Keywords:
Microscale
Jets
Channels
Viscous dissipation
Convective heat transfer
Scale-down limit

ABSTRACT

Classical heat transfer relations, claiming continual increase of cooling with downscaling, contradict previous experimental findings. We show that the reemergence of viscous dissipation at the microscale breaks heat transfer's symmetry and heat flux independence – the first such analysis for microjets. We also find that all bounded flows have maximal attainable cooling rates, corresponding to scale-down limits, given by a critical value of a new dimensionless group. While macro- and micro- dissipation are similar, their parameter ranges differ with jets introducing additional dependencies. This new micro-cooling performance envelope curbs the ongoing trend of flow miniaturization.

1. Introduction

Classical scaling laws for apparent *dimensionless* convective heat transfer coefficient (HTC) are traditionally independent of scale, implying ever increasing *dimensional* HTC, while decreasing the characteristic scale (d_h) and holding the dimensionless flow rate constant. However, this infinite trend seems physically unsound, and stands in contrast to previous experimental findings in channels of effective diameter below 100 μm [1–8]. We hereby show that viscous dissipation, though often overlooked, emerges due to high velocity gradients under down-scaling even in laminar flows [2], acting as a significant internal heat source which counteracts or even reverses this trend.

Although observed heat transfer reductions may be attributed to microscale-related measurement inaccuracies or heat loss uncertainty, they have been accredited to viscous dissipation both in theoretical [3] and numerical studies [4,5]. However, these studies did not identify the underlying heat transfer limits nor generalize dissipation's effect to bounded flows, as we present here. Considering the fluid as a continuum, it is seen to heat up internally due to viscous dissipation, thus the available for cooling capacity is reduced and vice versa for heating. This change in energy balance sets a *global* limit to attainable cooling and consequently, a limit to beneficial geometric scale-down. Indeed, already two decades ago it was noted that dissipation would dictate "… the fundamental limit to the reduction of the microchannel dimension…" [6]. In this letter, we characterize this fundamental limit and its dependencies on physical parameters for impinging jets, as well as finding similarity to all bounded flows, for the first time.

Traditionally, dissipation is considered in high-velocity compressible turbulent gas flows or high-viscosity liquid flows. For the latter, the ratio of viscous dissipation heating to imposed heating is termed the brinkman number [7] and its modification of the heat transfer has a standard form [4]:

$$\mathrm{Nu} = \mathrm{Nu_{ND}}\left(\frac{1}{1+f\,(\mathrm{Br})}\right) \quad \text{with} \quad \mathrm{Br} \equiv \frac{\rho\nu^3\mathrm{Re}^2}{q d_h^3}, \tag{1}$$

where the dimensionless HTC is $Nu = h{\cdot}d_h/k$ and h is the dimensional one given by Newton's law, $h \equiv q/(T\text{-}T_\infty)$ (where q is the imposed bounding wall heat flux and ΔT the resulting d_h is the hydraulic diameter (= 4 × crossectional area/perimeter), k is thermal conductivity, ρ is the fluid density, ν is kinematic viscosity and subscript ND for negligible dissipation conditions. Lastly, the dimensionless flow rate is defined by the Reynolds number $Re = u_m d_h/\nu$, where u_m is the mean inflow velocity.

Eq. 1 depicts the competition between dissipation and convective heat transfer studied here. Although dissipation can be sensitive to local surface conditions [8] and channel corner rounding [9], it is here *theoretically* analyzed under simple laminar flow conditions. Therein, dissipation occurs at the problem's characteristic scale (d_h) and not at the smallest turbulent vortex scale.

Compared to channel flows the more complex case of dissipation in jet impingement (see Fig. 1), has not been previously solved. Due to its inherently high heat transfer potential it is of special interest, is a prime candidate for miniaturization, and has been studied extensively by the authors [10–12]. Although dissipation in jets has been *experimentally* examined and significant HTC reduction found [13–15], this was with high viscosity fluids at the macro-scale. We herein theoretically extend the analysis of dissipation's influence beyond developed channel flows to the complex, archetypal configuration of jets, while focusing on the

* Corresponding author.
E-mail address: hermanh@post.tau.ac.il (H.D. Haustein).

https://doi.org/10.1016/j.icheatmasstransfer.2019.02.003

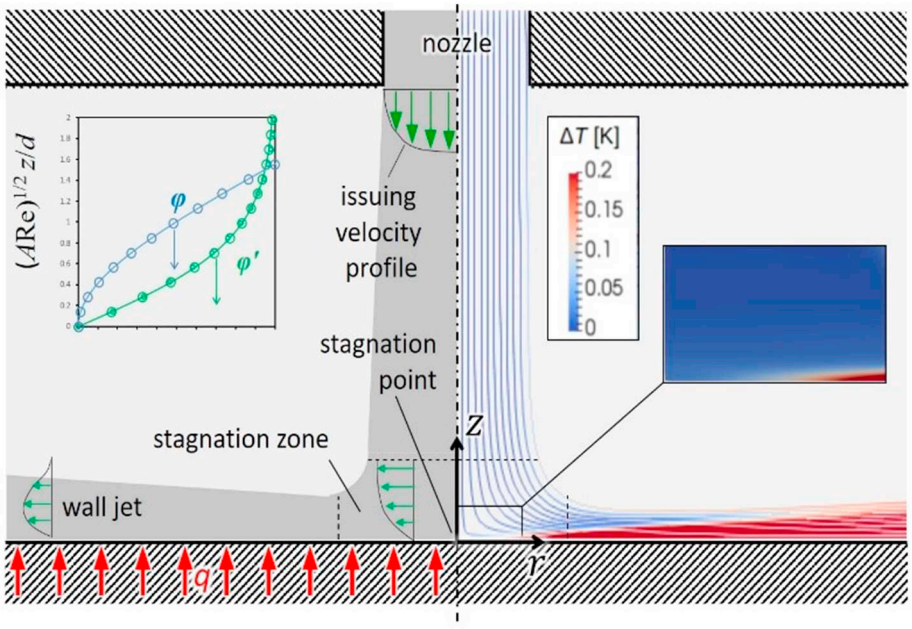

Fig. 1. Axisymmetric jet impingement. Left – Configuration schematic; inset = flow approximation, Eq. (4). Right – typical adiabatic-wall (q = 0) simulated thermal and flow fields: inset = close-up view of the impingement point; color = temperature, overlaid on streamlines.

microscale where the highest heat transfer can be found. Firstly, all derivations were validated against extensive numerical solutions of the full continuity, momentum, and energy equations. The analysis then enabled exploration of the diverse parametric space, showing new and unexpected trends. Moreover, it enabled generalization of findings to include known channel flow behavior, through a new dimensionless group.

2. Methods

2.1. Derivation

To analyze the effects of dissipation in jets, previously shown to maintain steady flow throughout the laminar range [16,17], we recall the *full* steady incompressible energy equation,

$$c_p(\mathbf{V}\cdot\nabla T) = \frac{k}{\rho}\nabla\cdot(\nabla T) + \underbrace{\nu\left(\frac{\partial u_i}{\partial x_j}+\frac{\partial u_j}{\partial x_i}\right)\frac{\partial u_i}{\partial x_j}}_{\Phi}, \tag{2}$$

where T and $\mathbf{V}$ are temperature and velocity fields (with components u_i); c_p and k are specific heat and thermal conductivity, respectively. Including the viscous dissipation term Φ, requires pre-knowledge of the flow field *gradients* – i.e. a complete solution of the momentum equation.

where T and $\mathbf{V}$ are scalar temperature and velocity vector fields with components u_i in directions x_i. To extend the analysis to the *developing* case of an impinging jet, the energy balance is simplified by analyzing it near the jet axis. In other words, as $r\to 0$: radial velocity is negligibly small and radial conduction is negligible relative to axial conduction, giving:

$$\rho\, c_p w\frac{\partial T}{\partial z} - k\frac{\partial^2 T}{\partial z^2} = 2\mu\left(\left(\frac{\partial u}{\partial r}\right)^2+\left(\frac{u}{r}\right)^2+\left(\frac{\partial w}{\partial z}\right)^2+\frac{1}{2}\left(\frac{\partial w}{\partial r}+\frac{\partial u}{\partial z}\right)^2\right) \tag{3}$$

Employing now Homann's classical solution for a jet's stagnation zone flow field allows further simplification. In Homann's work, the radial momentum balance was solved numerically in terms of the stream-function (φ), given in tabulated form in Schlichting [18]. The stream-function is defined so as to identically comply with the continuity equation (mass balance), in its role as a function primary to the velocity components according to $u_r \equiv -(\partial\varphi/\partial z)/r$ and $u_z \equiv (\partial\varphi/\partial r)/r$. However, the previous *tabulated* numerical solution does not support further analytical derivation, and is instead, approximated here as

$$\varphi = -\frac{u_m A r^2}{B\sqrt{A\,\mathrm{Re}}}\ln\left(\cosh\left(B\sqrt{A\,\mathrm{Re}}\,\frac{z}{d_h}\right)\right), \tag{4}$$

and its first derivative φ', as shown in the inset of Fig. 1. This approximation contains a single fit-parameter $B = 1.178$, balancing the requirements of fitting the radial and axial velocities as well as their gradients. Therein, it is seen that the best-fit for each gives a range of $B = 1.13$–1.2 – not far from the tabulated wall shear which requires $B = 1.312$. Additionally, A is the well-known dimensionless radial velocity gradient, which ranges $0.91 \le A \le 4.64$ – from uniform to parabolic profiles [19,20]. Note that this solution assumes $A = \partial u_r/\partial r$ is a constant dependent on the arriving profile but independent of r and is therefore only valid near the axis.

This new form is mathematically simpler and asymptotically more correct than a previous 3rd order polynomial approximation [21], somewhat similar to a recent wall-jet analysis [22]. Employing this approximation in the standard axisymmetric description gives

$$u_r = u_m A\frac{r}{d_h}\tanh\left(B\sqrt{A\,\mathrm{Re}}\,\frac{z}{d_h}\right)$$
$$u_z = -u_m\frac{2A}{B\sqrt{A\,\mathrm{Re}}}\ln\left(\cosh\left(B\sqrt{A\,\mathrm{Re}}\,\frac{z}{d_h}\right)\right)' \tag{5}$$

where u_m is the mean jet issuing velocity (see Fig. 1) and the viscous boundary layer height is defined by the radial velocity magnitude as:

$$\frac{\delta}{d_h} = \frac{\mathrm{arctanh}(0.99)}{B\sqrt{A\,\mathrm{Re}}}, \tag{6}$$

where the cut-off criterion is conventionally chosen as 99%.

Eq. (5) further reduces the complexity of the energy balance (Eq. (3)): as $\partial u_r/\partial r \equiv u_r/r$ – it allows joining the second term on the RHS with the first, by stating $w \neq w(r)$ it eliminates the one-before-last term and permits neglecting the last term as the only remaining r-dependent

one. Thereby reducing the energy balance to

$$k\frac{\partial^2 T}{\partial z^2} - \rho c_p u_z \frac{\partial T}{\partial z} = -2\rho\nu\left(2\left(\frac{\partial u_r}{\partial r}\right)^2 + \left(\frac{\partial u_z}{\partial z}\right)^2\right). \tag{7}$$

In the interest of proceeding analytically, one last simplification is required, i.e. the second term on the LHS is approximated under negligible dissipation conditions (subscript ND), in which case Eq. (7) becomes homogenous:

$$\left(k\frac{\partial^2 T}{\partial z^2}\right)_{\mathrm{ND}} - \left(\rho c_p u_z \frac{\partial T}{\partial z}\right)_{\mathrm{ND}} = 0 \tag{8}$$

Introducing this approximation back into Eq. (7) leads to:

$$k\frac{\partial^2 T}{\partial z^2} - \left(k\frac{\partial^2 T}{\partial z^2}\right)_{\mathrm{ND}} \cong -2\rho\nu\left(2\left(\frac{\partial u_r}{\partial r}\right)^2 + \left(\frac{\partial u_z}{\partial z}\right)^2\right). \tag{9}$$

In order to obtain the expression of the dissipation's heating *on the wall* the equation needs to be integrated over the characteristic *thermal transport scale*. Performing the integration and recognizing that $\partial T/\partial z|_{z=0} = h_{\mathrm{ND}}(T\text{-}T_\infty)$ with h_{ND} being dictated by the flow and independent of the thermal boundary condition near the axis [10]. Here it is understood that the conduction at the wall $k(\partial T/\partial z)_{z=0}$ is equal to the stagnation-point convection, $h_0(T\text{-}T_\infty)$, where the coefficient, $h_{0,}$ is a product of the flow field only and therefore independent of dissipation level.

The integration leads, in dimensionless terms, to a Brinkman-like parameter, which solely depends on viscous flow conditions and is independent from imposed heat flux:

$$\frac{1}{\mathrm{Br_D}} \equiv \frac{h_{\mathrm{ND}}\, d_{\mathrm{h}}^3 \overbrace{(T - T_{\mathrm{ND}})}^{\Delta T_{\mathrm{D}}}}{\rho\nu^3 \mathrm{Re}^2} = 2A^2\frac{\delta_{\mathrm{T}}}{d_{\mathrm{h}}}\left(1 - \frac{\frac{\delta}{\delta_{\mathrm{T}}}\tanh\left(\operatorname{arctanh}(0.99)\frac{\delta_{\mathrm{T}}}{\delta}\right)}{\operatorname{arctanh}(0.99)}\right). \tag{10}$$

Here the additional heating due to dissipation is seen to be dependent on incoming profile A, thermal boundary layer thickness δ_{T} and its ratio to the viscous boundary layer.

The ratio of viscous to thermal boundary layers is dependent on the corresponding ratio of diffusivities, i.e. on the Prandtl number ($Pr = \nu\rho c_p/k$) raised to a power known to vary from ½ to ⅓ as Pr goes from $Pr \ll 1$ to $Pr \gg 1$ (Schlichting [18]). Specifically, for stagnation flow the relation is given by White on page 183 [23] in a piece-wise manner, rewritten in normalized terms as:

$$\frac{\delta}{\delta_{\mathrm{T}}} = \begin{cases} \dfrac{1}{0.539}\dfrac{\sqrt{2\,\mathrm{Pr}/\pi}}{1 + 0.804552\sqrt{2\,\mathrm{Pr}/\pi}} & \mathrm{Pr} \le 0.15 \\ \mathrm{Pr}^{2/5} & 0.15 < \mathrm{Pr} < 3 \\ \dfrac{0.60105\mathrm{Pr}^{1/3} - 0.050848}{0.539} & \mathrm{Pr} \ge 3 \end{cases} \tag{11}$$

Introducing this relation into the expression for dissipation's wall heating together with an analytical submerged-jet heat transfer model for ($h_{\mathrm{ND}} = k\sqrt{2A\,\mathrm{Re}}\cdot 0.539\cdot\delta/(\delta_{\mathrm{T}}\cdot d)$ from [24]), allows prediction of $\mathrm{Br_D}$ over a wide range of conditions.

Furthermore, as will be shown in Section 3.1, by limiting the range of Pr, a *continuous* approximation to Eq. (11) can be employed without noticeable loss of accuracy. Thereby replacing both the need for the piece-wise description and conveniently leading to the standard form of heat transfer modification by dissipation (Eq. (1)), through the form:

$$\frac{1}{\mathrm{Br_D}} \cong 16\frac{A^{\frac{3}{2}}}{\mathrm{Re}^{\frac{1}{2}}\mathrm{Pr}^{\frac{2}{3}}}. \tag{12}$$

Up to this point, the derivation has been independent of the thermal boundary condition at the wall and is valid for both adiabatic and non-adiabatic cases. We now address the more relevant non-adiabatic, heat transfer case by superimposing the additional dissipative heating given in Eq. (10), on to the dissipation-free wall heat transfer. This is permitted, as the energy equation (Eq. (2)) is linear in T and the dissipation is its inhomogeneous part (see Appendix B of [25]).

It is thereby understood that with the significant dissipation an imposed heat flux q generates an *increased* temperature rise at the wall $\Delta T_{\mathrm{ND}} + \Delta T_{\mathrm{D}}$ and the effective heat transfer coefficient is reduced according to the ratio:

$$\left(\frac{h_{\mathrm{ND}}}{h}\right)_{q=const} = \frac{q}{\Delta T_{\mathrm{ND}}}\frac{(\Delta T_{\mathrm{ND}} + \Delta T_{\mathrm{D}})}{q} = 1 + \frac{\Delta T_{\mathrm{D}}}{\Delta T_{\mathrm{ND}}} \tag{13}$$

This can be rewritten in the standard form (Eq. (1)), similar to channel flows:

$$\frac{\mathrm{Nu}}{\mathrm{Nu_{ND}}} = \frac{1}{1 + \frac{\mathrm{Br}}{\mathrm{Br_D}}} \cong \frac{1}{1 + 16\frac{A^{3/2}\mathrm{Br}}{\mathrm{Re}^{1/2}\mathrm{Pr}^{2/3}}} \tag{14}$$

These newly derived expressions for dissipation's effect on the wall temperature, and consequently on heat transfer, will be tested and validated in Section 3.1 and 3.2 by comparison to detailed numerical simulations.

2.2. Numerical methods

In the present study we derived an analytical solution for viscous heating at the stagnation point of axisymmetric laminar jets. This derivation involved several simplifications and approximations, and therefore an extensive validation is presented here by comparing predictions to numerical solutions of the governing continuity, momentum (Navier-Stokes) and energy equations (Eqs. (15)–(17), respectively).

$$\nabla\cdot\mathbf{V} = 0 \tag{15}$$

$$(\mathbf{V}\cdot\nabla)\mathbf{V} = -\nabla p/\rho + \nu\nabla^2\mathbf{V} \tag{16}$$

$$c_p(\mathbf{V}\cdot\nabla T) = \frac{k}{\rho}\nabla\cdot(\nabla T) + \Phi \tag{17}$$

These equations were solved for a variety of flow and thermal conditions under three important assumptions, which reduce the number of problem parameters and increase the focus on the studied phenomenon: i) The flow is axisymmetric, laminar and steady, as observed in small diameter jets at $Re \le 2000$ [16,17]. Moreover, previous unsteady numerical simulations [12] revealed that despite initial vortices, a steady state is obtained after a short transient; ii) The fluid is considered to be Newtonian with constant thermophysical properties, as is generally acceptable for small thermal rises [10]; iii) The impinged solid surface is very thin, and therefore radial heat conduction in it is neglected relative to the convection from it.

We first solve the momentum equation and then the full axisymmetric energy equation as there is one-way coupling between them.

The numerical domain is presented in Fig. 2a. It is of rectangular shape with an axis of symmetry on the left hand side, jet inlet at the top and outlet on the right hand side, bounded by solid walls. The jet inlet to bottom wall spacing is three nozzle diameters, a value which balances minimal jet profile evolution during flight and unwanted confinement effects. The radial extent is eight diameters and was found in a previous study [12] to be sufficiently large to have a negligible effect on the flow in the vicinity of the stagnation point – the location which is the focus of this work.

No-slip boundary conditions were imposed at the two walls, and zero pressure at the outlet. At the inlet three different issuing profiles were imposed: uniform, partially-developed and fully-developed (parabolic), corresponding to $A \cong 1$, 2 and 4, respectively.

The coupling between pressure and velocity in the governing equations was resolved by the coupled scheme in the commercial solver ANSYS Fluent. All spatial discretization was of second order. The numerical domain was discretized with quadrilateral cells, consisting of

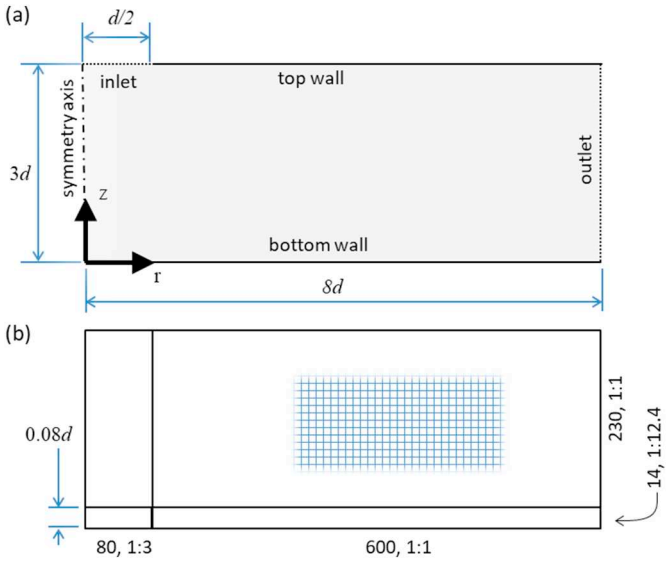

Fig. 2. The numerical domain and mesh.

four sub-domains, allowing cell size grading near the bottom wall and axis. The number of divisions and size ratios are given in Fig. 2b, and the total cell count is 166,000.

To verify independence of results from cell size, two additional meshes were prepared: a coarse mesh consisting of 41,500 cells, and a fine mesh, consisting of 664,000 cells. In Fig. 3 the impinged wall temperature distribution for two extreme cases and the three meshes are shown. Both cases are with an adiabatic wall boundary condition ($q = 0$) subject to high-flow viscous heating (Re = 1000) and are seen to be the most challenging numerically: at $Pr = 700$ the thinnest thermal boundary layer occurs, while at $A = 4$ the flow has the highest local velocities. The figure demonstrates that the initial mesh of 166,000 cells can be regarded as cell-size independent, even under these extreme conditions.

3. Results and discussion

This new solution is validated by comparison to extensive numerical simulations, and new findings are discussed. Starting with the simpler case of an adiabatic wall, the sole contribution of dissipation is evaluated. This is then followed by the more generally relevant non-adiabatic case with an imposed heat flux at the wall. Taking advantage of the new analytical solution, the parameter space is then explored. And finally, the findings are generalized to all bounded flows, including several types of channels, showing the similarities and differences between them.

3.1. Adiabatic wall case

This new solution is first validated in the simpler case of an adiabatic wall ($q = 0$) – a common experimental arrangement for isolating the influence of dissipation as the only heat source expressed through small, but measurable, wall temperature rise [14,15]. For these conditions the reference case (negligible dissipation) is isothermal, i.e. $T_{ND} = T_\infty$, and Eq. (10) together with the Pr dependence, Eq. (11), gives the entire wall temperature rise.

The new solution's prediction of the wall temperature rise was compared to extensive numerical results ($100 \le Re \le 2000$, $0.95 \le A \le 3.95$ and $0.1 \le Pr \le 100$), showing good agreement over two orders of magnitude of Br_D (not shown). An average deviation between them of 17.6% was found, when limiting the comparison to the range where the solution assumptions are valid, i.e. where nominal thermal and viscous boundary layers are of similar scale ($0.2 \le Pr \le 20$). Within this range convenient approximation (Eq. (12)) can be employed. At lower- and higher- Pr conditions under-prediction of the wall temperature occurs, due to two distinct causes: i) the emergence of heat sources outside the nominal thermal boundary layer which unexpectedly raise the wall temperature at high Pr; ii) at low-Pr (and low Peclet number, $Pe \equiv Re{\cdot}Pr \sim O(10)$) the neglected radial conduction reemerges and again raises wall temperate unexpectedly. The onset of streamwise conduction has been claimed to occur at similar Pe in pipe flows [26]. Moreover, its claimed increased-heating role is supported by the improved prediction found under *imposed* heat flux conditions (Fig. 5), which overshadows radial conduction.

3.2. Heat transfer case

Beyond the simple case of an adiabatic wall, this new approximate solution (Eq. (14)) for the heat transfer case is validated in detail against present numerical solutions in Fig. 4, for a range of diameters at an imposed heat flux typical to micro-electronics. The figure shows that despite the approximate nature of Eq. (14) it predicts HTC values and trend very well. The figure shows the expected break-away from macro-scale heat transfer (dashed line) under scale-down, occurring in given

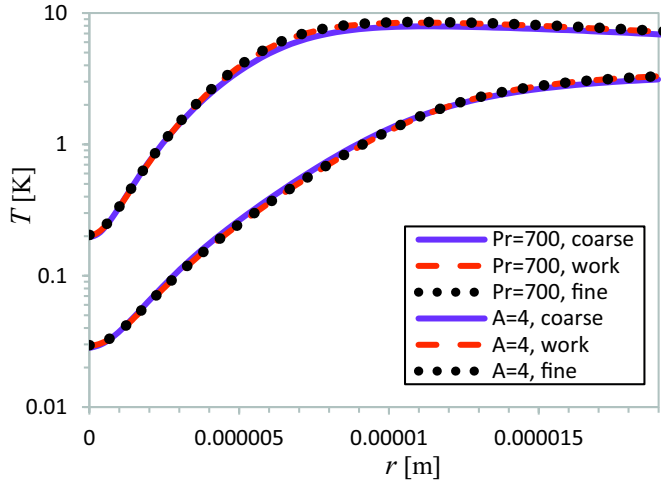

Fig. 3. Mesh independence test, showing independence for the working mesh even for two extreme cases (Re = 1000).

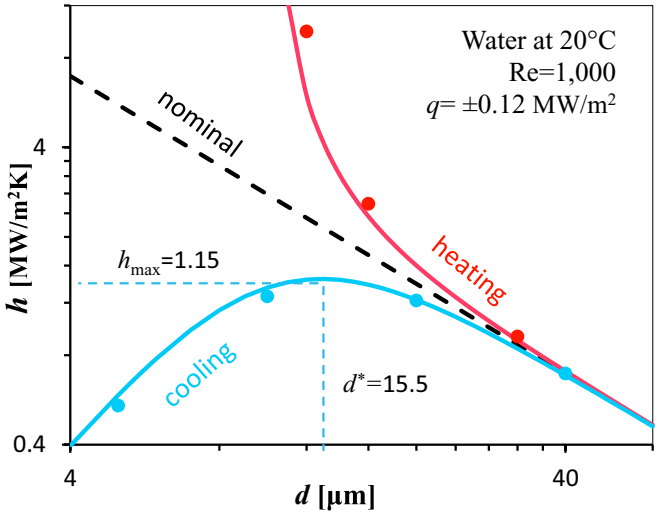

Fig. 4. Heat transfer reduction/increase due to dissipation under cooling/heating as dependent on jet size, present simulations vs. new model, Eq. (14).

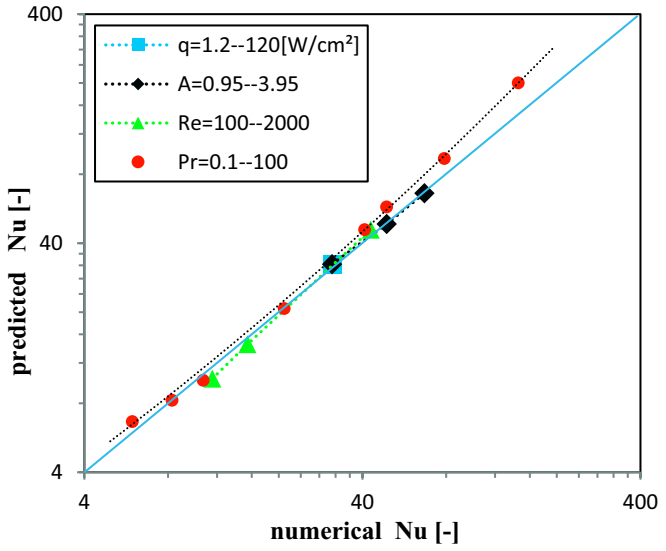

Fig. 5. Validation of the solution for heat transfer modified by dissipation – non-adiabatic-wall case under jet impingement, prediction by Eq. (14) compared to simulations over a wide range of conditions.

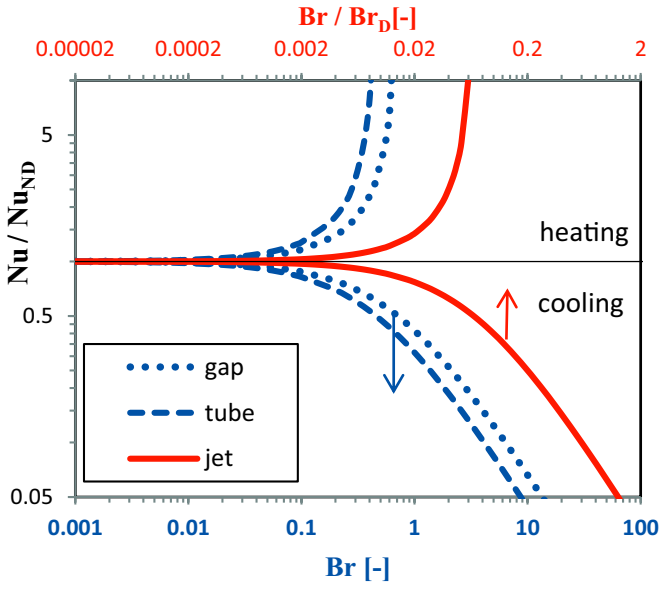

Fig. 6. Heat transfer modification by dissipation for three different cases, at both positive/negative heat fluxes – wall cooling/heating; compared to simulations (q = 0.12 MW/m^2 water microjet at 20 °C, at Re = 1000; issuing with a uniform profile A = 0.95).

dimensional terms at around 50 μm, for both *heated* and *cooled* wall conditions. This break-away reveals three new features: i) A distinct lack of symmetry between the cooling and heating cases resulting in effective decreased/increased HTC; ii) HTC's value becomes dependent on heat flux, e.g. in the wall cooling case an increase in the imposed heat flux will lead to an increase in apparent HTC; iii) In the cooling case, the effective HTC obtains a maximal value, h_{max} at an optimal diameter, d^*, (values given in the figure). This maximum indicates a point at which dissipation overcomes the inherent increase of dimensional HTC with scale-down. All these features contradict known single-phase flow HTC behavior – which is nominally linearly dependent on scale, and independent of the value and sign of imposed heat flux.

In the light of the maximum shown in Fig. 4, further validation of Eq. (14) was conducted at the critical diameter – where a significant

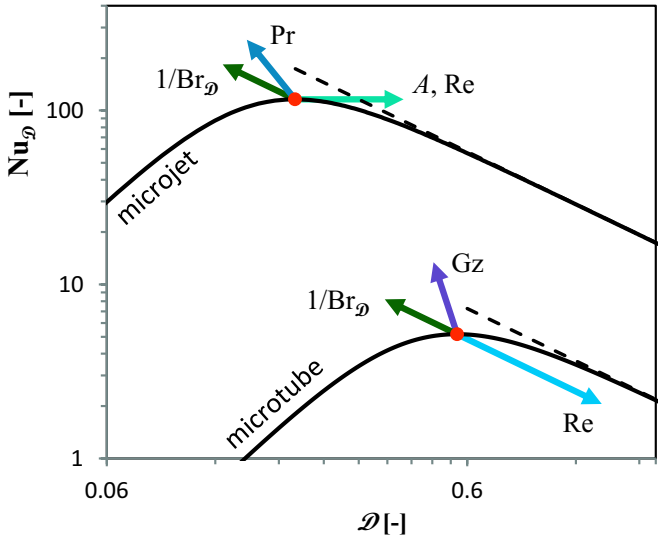

Fig. 7. Dependence of heat transfer on scale for microjet (A = 1) and microtube (solid line is water entering at 20 °C, Re = 500 and q equal to Fig. 4 and equivalent to Br$_{\mathcal{D}}$ = 0.02). Red dots mark critical points, and arrows indicate their displacements, resulting from exclusive 4-fold variation in all parameters except Gz which varies from 0 to 500. (For interpretation of the references to color in this figure legend, the reader is referred to the web version of this article.)

effect of dissipation is to be found. Again, comparison to numerical simulations over a wide range of conditions showed even *better* agreement than the adiabatic case ($0.1 \le Pr \le 100$, $100 \le Re \le 2000$, $0.012 \le q \le 1.2$MW/m^2, $0.95 \le A \le 3.95$). This improved agreement over an extended range (average error = 9.4%, $0.1 \le Pr \le 100$) is shown in Fig. 6. Thereby, not only do predictive errors appear reduced, but especially low-Pr predictions improve. This can be understood as the prediction error of the dissipation heat up only modifies the already well-predicted Nu_{ND}. The accuracy is improved in the low-Pr range, where the detrimental radial conduction is overtaken and effectively suppressed by the imposed heat flux, thus complying better with the assumptions made in the solution derivation. Note that the variation of q involves a corresponding variation in d_h in order to remain at the maximum heat transfer, resulting in an independence of Nu from q. However, if d_h were held constant the dependence of Nu on q would be seen.

3.3. Generalization of findings

The inherent similarities and differences between jets and other channel flow configurations are considered in the following. First, the modification of heat transfer by dissipation according to Eq. (14) is compared, in dimensionless terms, to previous solutions of two basic channel configurations [4,27], as shown in Fig. 6. The similarity between channels and jets is immediately obvious under both heating and cooling constraints, though different scaling is required for each. While the difference between tubes and gaps is only a constant factor, the jet involves additional dependence on the issuing profile, fluid properties, and flow rate (*A*, Pr and Re, respectively). Due to these additional dependencies, multiple pathways may lead to identical levels of dissipation. For instance, if the flow rate is represented by Re, the nozzle geometry by *A*, and the liquid properties by Pr, then Br can be seen to represent the characteristic scale at a given imposed heat flux, spanning a very wide and independently variable parametric space.

The similar trends of jets, gaps, and tubes, including thermally developing conditions in tubes [28] (recently correlated by the authors [29]), indicate that it may be possible to formulate a single equation, generalizing all known cases. We therefore rewrite Eq. (14) in a more

general form as

$$\frac{\mathrm{Nu}}{\mathrm{Nu_{ND}}} = \frac{1}{1 + \underbrace{\frac{\mathrm{Br}}{\mathrm{Br_D}} - \frac{24(\pi+3)}{110}\sum_{j=1}^{N}\frac{e^{-4j(8j+5)/\mathrm{Gz}}}{j^2}\left(\mathrm{Br} + \frac{\pi\sqrt{j}}{10}\right)}_{\equiv\mathcal{B}}} \tag{18}$$

where $\mathcal{B}$ is a new dimensionless group encompassing the modification of heat transfer due to dissipation, and Gz is the well-known Graetz number (inverse of the thermal length scale, $\mathrm{Gz} \equiv \mathrm{Pe}\cdot d_h/z$). This new group is defined so as to cover all cases and will be shown to obtain a critical value at the heat transfer maximum. Therein, each configuration experiences a reduction of its known $\mathrm{Nu_{ND}}$, through its modification by $\mathrm{Br_D}$ and/or Gz. The latter parameter plays a role in $\mathcal{B}$ only for finite Gz, i.e. only for the thermally developing flow in a tube. For the case of jets, $\mathrm{Br_D}$ is given by Eq. (10) or approximately by Eq. (12), while for tubes $\mathrm{Br_D} = 11/48$ ($\mathrm{Nu_{ND}} = 48/11$) and for gaps $\mathrm{Br_D} = 17/48$ ($\mathrm{Nu_{ND}} = 140/17$) [30].

Unfortunately, the standard dimensionless representation of Fig. 6 fails to exhibit the inherent dimensional cooling limit pursued here (and shown in Fig. 4). Focusing on the significant cooling reduction encountered during scale-down, an *independent* scale is seen to be required in order to express the microscale effects. Therefore, a scale related to thin-film flows is hereafter employed – $\mathcal{D} \equiv d_h/(\nu^2/g)^{1/3}$, leading to alternative dimensionless definitions for heat transfer and imposed heat flux, $\mathrm{Nu}_\mathcal{D} \equiv \mathrm{Nu}/\mathcal{D}$ and $\mathrm{Br}_\mathcal{D} \equiv \mathrm{Br}\cdot\mathcal{D}^3$. Use of the new definitions in Eq. (18), gives the curves shown in Fig. 7. Therein, the conditions for the microjet flow were chosen at the center of the valid parametric space, identified from the non-adiabatic case study (as listed in the caption). The figure demonstrates that with scale-down, for all of the considered cooling flow types, heat transfer breaks away from its well-known, dissipationless linear dependence (dashed line), eventually attaining a maximum in the $\mathcal{D}$–$\mathrm{Nu}_\mathcal{D}$ plane. This is the point at which dissipation's heating overcomes convection and is therefore the maximal obtainable cooling rate, which occurs at a critical diameter $\mathcal{D}^*$ – the absolute limit to beneficial scale-down.

Subsequent analysis revealed that the maximal heat transfer is two-thirds of the nominal one ($\mathrm{Nu}_{\mathcal{D},\max} = \frac{2}{3}\cdot\mathrm{Nu_{ND}}/\mathcal{D}$) at a critical flow-diameter, given by:

$$\mathcal{B}^* \equiv \mathcal{B}(\mathcal{D}^*) = \frac{1}{2}. \tag{19}$$

Introducing the appropriate values of $\mathrm{Br_D}$ and Gz into $\mathcal{B}^*$ for each case, reveals the different dependencies of the critical scale and maximal heat transfer (see arrows and caption in Fig. 7). While microgaps behave similarly to microtubes and are therefore not shown, jets exhibit a higher maximum under identical constraints. On the one hand, all cases have a common dependence on $\mathrm{Br}_\mathcal{D} \propto 1/q$, which displaces the maximum parallel to the dissipationless trend (dashed line). While on the other, jets' additional dependencies on Pr, and A and thermal development in microtubes' dependence on Gz shift the maximum in new directions. Furthermore, while both cases share a dependence on Re, they differ in directions.

4. Conclusions

By dealing with significant viscous dissipation occurring at high pressure drops [31], the present study identifies the heat transfer *performance envelope*, already within reach of many applications. Examining three configurations (jets, gaps and tubes) with various liquids, flow rates, and under typical microelectronics cooling constraints (inlet at 20 °C with outlet ≤80 °C) gave a wide range of maximum HTCs, $h_{\max}$~O(10^3–10^7) W/m^{2}K, with a critical diameter range of $d^* = 2$–$30\,\mu$m. Although these scales may seem very small, they are already becoming relevant [32] and will increase with tighter thermal constraints (permisible q). Furthermore, as significant deviation from nominal heat transfer begins already around three times the critical diameter, it is recommended that high-Re micro-flows, $d_h \le 100\,\mu$m, consider dissipation along the lines shown here.

In this novel study, we have examined the effects of scale-down and confinement, which is of increasing recent interest. Therein, we quantified the importance of viscous dissipation for impinging jets at the microscale for the first time and compared it to previous analysis of microtubes and microgaps. Our analysis shows that all flows behave similarly, though jets encompass more complex scaling. Furthermore, dissipation causes a breaking of heat transfer's inherent symmetry and independence from heating level, in all cases. These understandings apply to larger scales too, as dissipation in both macro- and microflows is expressed through Br. However, macro *liquid* flows are dominated by high-viscosity, whereas, due to their scale, microflows may encounter significant dissipation and heat transfer modification even at low Pr. Moreover, we show that a unified dimensionless form can be formulated for all known cases, leading to the emergence of the new dimensionless group $\mathcal{B}$. By analyzing this unified form using an independent characteristic scale, down-scaling effects could be studied. Therein, we have revealed a peak in the attainable cooling for all cases, corresponding to a critical value of the new dimensionless group ($\mathcal{B}^* = 1/2$). This maximum is attained at a critical flow diameter, which is the effective scale-down limit for micro cooling flows. Although this scale-down limit has previously been contemplated, it has been analyzed and quantified here for the first time.

Most importantly, we have characterized and quantified the **absolute limits** of single-phase convective cooling, thereby quantifying the **remaining potential** for improvement through down-scaling. The performance envelope we have outlined here **restrains the ongoing trend** of cooling-flow miniaturization. Finally, the present findings provide a framework for analyzing more complex cases, including temperature dependent fluid properties, mass transfer equivalent cases and more complex reactive flows.

Acknowledgements

We acknowledge the support of the Israel Science Foundation grant 4112/17 and initiation of this debate by their reviewers.

References

[1] A. Bucci, G.P. Celata, M. Cumo, E. Serra, G. Zummo, Water Single-Phase Fluid Flow and Heat Transfer in Capillary Tubes, 1st Int. Conf. Microchannels Minichannels, (2003), pp. 319–326.
[2] P. Rosa, T.G. Karayiannis, M.W. Collins, Single-phase heat transfer in microchannels: the importance of scaling effects, Appl. Therm. Eng. 29 (17–18) (2009) 3447–3468.
[3] G.L. Morini, Scaling effects for liquid flows in microchannels, Heat Transf. Eng. 27 (4) (2006) 64–73.
[4] H.E. Jeong, J.T. Jeong, Extended Graetz problem including streamwise conduction and viscous dissipation in microchannel, Int. J. Heat Mass Transf. 49 (2006) 2151–2157 (13–14).
[5] J. Koo, C. Kleinstreuer, Viscous dissipation effects in microtubes and microchannels, Int. J. Heat Mass Transf. 47 (14–16) (2004) 3159–3169.
[6] C.P. Tso, S.P. Mahulikar, The use of the Brinkman number for single phase forced convective heat transfer in microchannels, Int. J. Heat Mass Transf. 41 (12) (1998) 1759–1769.
[7] H.C. Brinkman, Heat effects in capillary flow I, Appl. Sci. Res. 2 (1) (1951) 120–124.
[8] G. L. Morini, Pressure-driven single-phase liquid flows, in Encyclopedia of Microfluidics and *Nanofluidics*, D. Li, Ed. New York, NY: Springer New York, 2015, 2846–2861.
[9] M. Lorenzini, N. Suzzi, The influence of geometry on the thermal performance of microchannels in laminar flow with viscous dissipation, Heat Transf. Eng. 37 (13–14) (2016) 1096–1104.
[10] W. Rohlfs, H.D. Haustein, O. Garbrecht, R. Kneer, Insights into the local heat transfer of a submerged impinging jet: influence of local flow acceleration and vortex-wall interaction, Int. J. Heat Mass Transf. 55 (25–26) (2012) 7728–7736.
[11] H.D. Haustein, J. Joerg, W. Rohlfs, R. Kneer, Influence of micro-scale aspects and jet-to-jet interaction on free-surface liquid jet impingement for micro-jet array cooling, Thermomechanical Phenomena in Electronic Systems -Proceedings of the Intersociety Conference, 2014, pp. 904–911.
[12] B. Kashi, H.D. Haustein, Dependence of submerged jet heat transfer on nozzle length, Int. J. Heat Mass Transf. 121 (2018) 137–152.

[13] D.E. Metzger, K.N. Cummings, W.A. Ruby, Effects of Prandtl number on heat transfer characteristics of impinging liquid jets, in *Proceedings of the Fifth International Heat Transfer Conference* 2 (1974) 20–24.
[14] C.F. Ma, Q. Zheng, S.C. Lee, Impingement heat transfer and recovery effect with submerged jets of large Prandtl number liquid - I. Unconfined circular jets, Int. J. Heat Mass Transf. 40 (6) (1997) 1481.
[15] C.F. Ma, Q. Zheng, H. Sun, K. Wu, T. Gomi, B.W. Webb, Local characteristics of impingement heat transfer with oblique round free-surface jets of large Prandtl number liquid, Int. J. Heat Mass Transf. 40 (10) (1997) 2249–2259.
[16] W. Rohlfs, J. Jorg, C. Ehrenpreis, M. Rietz, H.D. Haustein, R. Kneer, Flow Structures and Heat Transfer in Submerged and Free Laminar Jets, in *Proceedings of the 1st Thermal and Fluids Engineering Summer Conference, TFESC-1*, (2015), pp. 1–21.
[17] B. Kashi, E. Weinberg, H.D. Haustein, Aanlytical re-examination of the submerged laminar jet's velocity evolution, Phys. Fluids 30 (2018) 063604.
[18] H. Schlichting, Boundary Layer Theory, 7th ed, McGRAW-HILL BOOK COMPANY, 1967.
[19] H. Martin, Heat and mass transfer between impinging gas jets and solid surfaces, Adv. Heat Transf. 13 (1977) 1–60.
[20] J.H. Lienhard, Liquid jet impingement, Annu. Rev. Heat Transf. (1995) 199–270.
[21] J. Pretsch, The Stability of Laminar Flow Past a Sphere, (1942).
[22] L.F. Mo, R.X. Chen, Y.Y. Shen, Application of the method of weighted residuals to the Glauert-jet problem, Phys. Lett. Sect. A Gen. At. Solid State Phys. 369 (5–6) (2007) 476–478.
[23] F.M. White, I. Corfield, Viscous Fluid Flow, vol. 3, McGraw-Hill New York, 2006.
[24] X. Liu, L.A. Gabour, J.H. Lienhard, Stagnation-point heat transfer during impingement of laminar liquid jets : analysis including surface tension, J. Heat Transf. 115 (February) (1993) 99–106.
[25] J. Holman, Heat transfer, Mc Graw Hill, (2010), 758.
[26] D.K. Hennecke, Heat transfer by Hagen-Poiseuille flow in the thermal development region with axial conduction, Wärme- und Stoffübertragung 1 (3) (1968) 177–184.
[27] O. Aydin, M. Avci, Viscous-dissipation effects on the heat transfer in a Poiseuille flow, Appl. Energy 83 (5) (2006) 495–512.
[28] T. Basu, D.N. Roy, Laminar heat transfer in a tube with viscous dissipation, Int. J. Heat Mass Transf. 28 (3) (1985) 699–701.
[29] H.D. Haustein, B. Kashi, The Importance of Viscous Dissipation in Micro-Tube and Micro-Gap Flows, in *5th Internationa1 Conference on Nano- Micro- Mini-channels, ICNMM2018*, (2018).
[30] V.W. Schach, Umlenkung eines kreisförmigen Flüssigkeitsstrahles an einer ebenen Platte senkrecht zur Strömungsrichtung, Ingenieur-Archiv VI Band 5 (1916) (1935) 51–59.
[31] J. Judy, D. Maynes, B.W. Webb, Characterization of frictional pressure drop for liquid ows through microchannels, Int. J. Heat Mass Transf. 45 (2002) 3477–3489.
[32] T. Brunschwiler, et al., Direct liquid jet-impingement cooling with micronsized nozzle array and distributed return architecture, Thermomechanical Phenom. Electron. Syst. -proceedings Intersoc, Conf. 2006 (May) (2006) 196–203.